Journal of Engineering Physics and Thermophysics, Vol. 70, No. 3, 1997

REVIEW

HEAT TRANSFER AND HYDRODYNAMICS IN CHANNELS ROTATING ABOUT THEIR AXIS

I. V. Shevchuk and A. A. Khalatov

UDC 532.5 + 536.24

Introduction. Axial rotating channels are widespread in power engineering industry, heat power engineering, power engineering, chemical engineering, aircraft engines, space systems, etc. Predominantly they are cylindrical in shape. Converging and diverging axisymmetric channels as well as channels of arbitrary shape are often used. The angular rotational velocity, which, in the general case, can be variable with time, is made constant in the majority of works. It is rotation that has a substantial effect on the characteristics of flow and heat transfer, changing (increasing or decreasing depending on the type of flow) the values of the heat-transfer coefficient and coefficient of hydraulic resistance by a factor of 2–3 or more. Much attention has been paid recently to investigating the action of additional complicating factors – injection or suction, the form of the inlet velocity profile, the disposition of the channel, etc. Several works are concerned with relatively infrequent problems of the flow of a liquid that occupies partially the cross-section of the channel, flow in a tube that is closed at one end, etc.

1. Horizontal Rotating Tube. Mathematical Description. To describe transfer processes in straight tubes of a constant circular cross section, a cylindrical coordinate system is used. In all the works that we know, it is fixed. Due to this rotational effects do not appear in the equations of motion in explicit form and act only indirectly through the influence of the boundary condition on a rotating wall as well as in terms of turbulence characteristics.

In what follows cylindrical coordinates are used; the zero value of the radial coordinate r coincides with the tube axis, that of the axial coordinate z, with the inlet section, and the zero value of the angular coordinate φ, with the vertical section of the tube. In this coordinate system, the equations of motion and energy have the following form:

$$\rho\left(\frac{\partial u_r}{\partial t}+u_r\frac{\partial u_r}{\partial r}+\frac{u_\varphi}{r}\frac{\partial u_r}{\partial \varphi}-\frac{u_\varphi^2}{r}+u_z\frac{\partial u_r}{\partial z}\right)=F_r-$$

$$-\frac{\partial p}{\partial r}+\mu\left(\nabla^2 u_r-\frac{u_r}{r^2}-\frac{2}{r^2}\frac{\partial u_r}{\partial \varphi}\right)+\frac{1}{r}\frac{\partial}{\partial r}\left(-\rho\overline{u_r'^2}\right)+$$

$$+\frac{1}{r}\frac{\partial}{\partial \varphi}\left(-\rho\overline{u_r'u_\varphi'}\right)+\frac{\partial}{\partial z}\left(-\rho\overline{u_r'u_z'}\right)-\frac{1}{r}\left(-\rho\overline{u_r'^2}\right); \qquad (1)$$

$$\rho\left(\frac{\partial u_\varphi}{\partial t}+u_r\frac{\partial u_\varphi}{\partial r}+\frac{u_\varphi}{r}\frac{\partial u_\varphi}{\partial \varphi}+\frac{u_r u_\varphi}{r}+u_z\frac{\partial u_\varphi}{\partial z}\right)=$$

$$=F_\varphi-\frac{1}{r}\frac{\partial p}{\partial \varphi}+\mu\left(\nabla^2 u_\varphi+\frac{2}{r^2}\frac{\partial u_\varphi}{\partial \varphi}-\frac{u_\varphi}{r^2}\right)+\frac{\partial}{\partial r}\left(-\rho\overline{u_r'u_\varphi'}\right)+$$

Institute of Technical Thermal Physics, National Academy of Sciences of Ukraine, Kiev. Translated from Inzhenerno-Fizicheskii Zhurnal, Vol. 70, No. 3, pp. 514-528, May-June, 1997. Original article submitted July 15, 1995.

1062-0125/97/7003-0511$18.00

$$+\frac{1}{r}\frac{\partial}{\partial\varphi}\left(-\rho\overline{u_\varphi'^2}\right)+\frac{\partial}{\partial z}\left(-\rho\overline{u_r'u_z'}\right)+\frac{2}{r}\left(-\rho\overline{u_r'u_\varphi'}\right); \tag{2}$$

$$\rho\left(\frac{\partial u_z}{\partial t}+u_r\frac{\partial u_z}{\partial r}+\frac{u_\varphi}{r}\frac{\partial u_z}{\partial\varphi}+u_z\frac{\partial u_z}{\partial z}\right)=F_z-\frac{\partial p}{\partial z}+$$

$$+\mu\nabla^2u_z+\frac{1}{r}\left(-\rho r\overline{u_r'u_z'}\right)+\frac{\partial}{\partial z}\left(-\rho\overline{u_z'^2}\right)+\frac{1}{r}\frac{\partial}{\partial\varphi}\left(-\rho\overline{u_\varphi'u_z'}\right); \tag{3}$$

$$\frac{\partial}{\partial r}(ru_r)+\frac{1}{r}\frac{\partial}{\partial\varphi}(ru_\varphi)+\frac{\partial}{\partial z}(ru_z)=0; \tag{4}$$

$$\rho C_p\left(\frac{\partial T}{\partial t}+u_r\frac{\partial T}{\partial r}+\frac{u_\varphi}{r}\frac{\partial T}{\partial\varphi}+u_z\frac{\partial T}{\partial z}\right)=$$

$$=\frac{1}{r}\frac{\partial}{\partial r}\left[r\left(\lambda\frac{\partial T}{\partial r}-\rho C_p\overline{u_r'T'}\right)\right]+\frac{\partial}{\partial z}\left(\lambda\frac{\partial T}{\partial z}-\rho C_p\overline{u_z'T'}\right)+$$

$$+\frac{1}{r^2}\frac{\partial}{\partial\varphi}\left(\lambda\frac{\partial T}{\partial\varphi}-\rho C_p\overline{ru_\varphi'T'}\right), \tag{5}$$

where

$$\nabla^2=\frac{\partial^2}{\partial r^2}+\frac{1}{r}\frac{\partial}{\partial r}+\frac{1}{r^2}\frac{\partial^2}{\partial\varphi^2}+\frac{\partial^2}{\partial z^2}.$$

In the majority of works, the stationary problem (ω = const) is investigated, which signifies $\partial/\partial t=0$. The boundary-layer approximation describes well flow in a rotating axial tube, which signifies $\partial^2/\partial z^2=0$ [1-11]. For an axisymmetric case, $\partial/\partial\varphi=\partial^2/\partial\varphi^2=0$ [1-8, 11]. Terms that contain derivatives of pulsation components with respect to z and φ are usually discarded because of their minor contribution. For the region of developed turbulent flow, the left-hand sides of Eqs. (1)-(3) and (5), except the term $\rho u\varphi^2/r$ in (1) and $\rho C_p u_z\partial T/\partial z$ in (5), are considered as equal to zero, the continuity equation (4) taking a simple form: $u_r=0$.

As has been noted above centrifugal and Coriolis forces do not enter in Eqs. (1)-(3) in explicit form. In [9, 10], the influence of buoyancy forces in a gravitational field for a laminar regime of flow is investigated. In this case, in Eqs. (1) and (2) there appear non-zero components of mass forces F_r and F_φ that have the following form:

$$\frac{F_\varphi}{\rho u_{z\,\mathrm{av}}^2/r_\mathrm{w}}=\frac{1}{2}\frac{\mathrm{Gr}}{\mathrm{Re}^2}\Theta\sin\varphi,\quad\frac{F_r}{\rho u_{z\,\mathrm{av}}^2/r_\mathrm{w}}=-\frac{1}{2}\frac{\mathrm{Gr}}{\mathrm{Re}^2}\Theta\cos\varphi,$$

where the temperature difference in the Grashof number is determined as $\Delta T=T_\mathrm{w}-T_{\max}$.

Boundary conditions on the wall are the equalities $u_z=u_r=0$ and $u_\varphi=u_\omega=\omega r$ as well as the prescribed heat flux or temperature (usually constant ones). On the tube axis, $\partial T/\partial r=0$, $u_r=u_\varphi=0$, and $\partial u_z/\partial r=0$. The velocity, temperature, and pressure distributions are prescribed at the inlet to the tube.

To close the system (1)-(5), the equations of the transfer of the pulsations $\overline{u_z'^2}$, $\overline{u_r'^2}$, $\overline{u_\varphi'^2}$, $\overline{u_z'u_r'}$, $\overline{u_z'u_\varphi'}$, $\overline{u_r'u_\varphi'}$, $\overline{u_z'T'}$, $\overline{u_r'T'}$, and $\overline{u_\varphi'T'}$ as well as ε, the rate of dissipation for the turbulent kinetic energy k_i, are used in [5, 6, 12]. In [5, 13, 14], a simpler k–ε model is employed, while in [2] differential equations for k and $\overline{T'^2}$ are solved that are used then to calculate $\overline{u_z'u_r'}$ and $\overline{u_r'T'}$ (the remaining pulsation components are not allowed for).

In [3, 7, 8], to calculate the pulsation $\overline{u_z'u_r'}$ (the remaining ones are considered negligibly small), the mixing length model is used

$$\overline{u_z' u_r'} = l^2 \left[\left(\frac{\partial u_z}{\partial r} \right)^2 + \left(r \frac{\partial}{\partial r} \left(\frac{u_\varphi}{r} \right) \right)^2 \right]^{1/2} \frac{\partial u_z}{\partial r}. \tag{6}$$

The quantity l is calculated in a form proposed by P. Bradshaw [15]:

$$l = l_0 (1 - \beta \, \mathrm{Ri})^m, \tag{7}$$

where l_0 refers to the fixed tube while the Richardson number is calculated by the formula for two-dimensional flows

$$\mathrm{Ri} = 2 \frac{u_\varphi}{r^2} \frac{\partial (u_\varphi r)}{\partial r} \Big/ \left[\left(\frac{\partial u_z}{\partial r} \right)^2 + \left(r \frac{\partial}{\partial r} \left(\frac{u_\varphi}{r} \right) \right)^2 \right]. \tag{8}$$

In [7], $m = 1$, $\beta = 0.4$ or 0.5 are used; in [8, 10, 11] – $m = 2$, while $\beta = 1/6$ – for the region of steady-state turbulent flow. In [3], $\beta = 2$ and 2.5 is realized on the initial segment of the tube. In [7], for a laminar flow that is turbulized by the rotation of the tube: $l/l_0 = 0.012 \mathrm{Re}_\omega^{0.5}$.

An approximate integral method for calculating friction and heat transfer is proposed in [16]. V. V. Novozhilov's model of turbulence is employed in [4] for this type of flow; the calculation errors are rather high.

For the characteristic of the influence of rotation on hydrodynamics and heat transfer, the Reynolds rotational number Re_ω and the simplex

$$N = \frac{u_\omega}{u_{z\,\mathrm{av}}} = \frac{\omega r_w}{u_{z\,\mathrm{av}}}.$$

are used.

For the region of steady-state turbulent flow, the authors of [11] obtained the parameter

$$Z = N \frac{\mathrm{Re}}{2 \mathrm{Re}_\tau} = \frac{u_\omega}{u_\tau} = N \left(\frac{\lambda_{\mathrm{hydr}}}{8} \right)^{-1/2}, \tag{9}$$

which permitted determination of a universal dependence for the axial component of the velocity.

Stability and Flow Regimes. The results of theoretical and experimental works [17-22] show that laminar flow is unstable to small nonviscous disturbances induced by the rotation of the tube about its axis. This instability manifests itself even for $\mathrm{Re} = 165.75$ and $\mathrm{Re}_\omega = 53.92$. Conversely, turbulent flow stabilizes as a whole in tube rotation, which is due to the conservative action of mass forces [1-8, 10-12, 14, 16, 21, 23-34].

As of now, the boundaries of flow regimes have been found only approximately. The principal criterion for their determination is the change in the overall coefficient of the tube's hydraulic resistance [1, 29]

$$\lambda_{\mathrm{hydr}} = \frac{\Delta p}{\rho u_{z\mathrm{av}}^2} \frac{2d}{L}.$$

When $\mathrm{Re} < 2 \cdot 10^3$ an increase in N leads to an increase in λ_{hydr}; as Re increases λ_{hydr} decreases, as it does in laminar flow in fixed tubes. This flow regime is called by V. K. Shchukin "disturbed laminar" [1]. For a transient flow regime (in the range $\mathrm{Re} = 2 \cdot 10^3 - 6 \cdot 10^3$), data for the dependence $\lambda_{\mathrm{hydr}}(\mathrm{Re}, \mathrm{Re}_\omega)$ are contradictory. A further increase in the number Re is characterized by curves for λ_{hydr} that have a minimum (extremum), the lines passing one below another as N increases [1, 29]. The point of the minimum depends on the numbers Re and Re_ω. Shchukin calls the flow in the Re number range from $6 \cdot 10^3$ to the minimum "laminarized" [1]. In this regime, the mass forces laminarize the flow but do not eliminate the remanent turbulence, due to which λ_{hydr} in this regime is higher than in laminar flow.

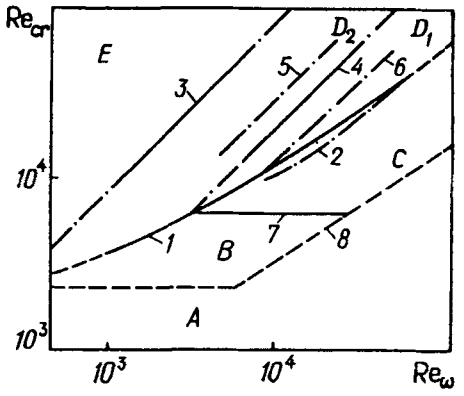

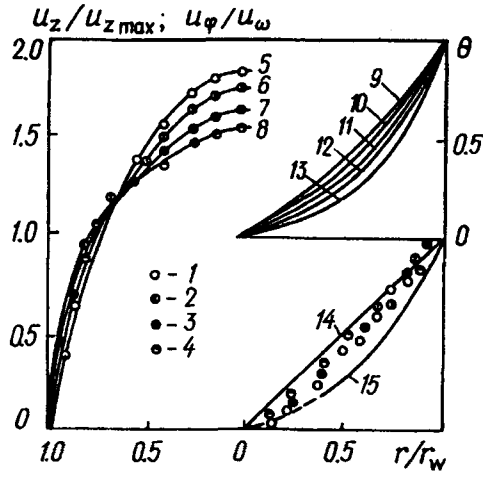

Fig. 1. Regions of flow regimes in axial rotating tube: 1) formula (10), 2) (11), 3) $N = 0.125$, 4) 0.475, 5) 0.35, 6) 0.8, 7) $Re_{cr} = 6 \cdot 10^3$, 8) boundary of disturbed laminar flow.

Fig. 2. Velocity and temperature profiles for laminar flow in axial rotating tube (Re = 1000): 1-4) experiment for $u_z/u_{z\,max}$ and u_φ/u_ω [7], 5-8) calculation for $u_z/u_{z\,max}$ [7], 9-13) calculation of Θ [9], 14) $u_\varphi/u_\omega = r/r_w$, 15) $u_\varphi/u_\omega = (r/r_w)^2$, 9) $Re_\omega = 0$; 1, 5, 10) 500; 2, 6, 11) 1000; 3, 7, 12) 1500; 4, 8, 13) 2000.

The increase in λ_{hydr} as Re increases further is due to changing over to turbulent flow that is subject to a conservative influence of rotation. V. K. Shchukin calls this regime "partially suppressed turbulent" [1].

For high Re numbers, the influence of rotation on the flow becomes secondary; the turbulent flow regime sets in. From the data of [1], here $\lambda_{hydr} = \lambda_{hydr.0}$ while from the data of [29] λ_{hydr} is somewhat larger, which is an error: the authors of [29] did not eliminate from λ_{hydr} the hydraulic resistance of the pre- and post-embedded fixed segments in which the sensors were located ($\lambda_{hydr.0}$ is the coefficient of hydraulic resistance for the fixed tube).

The dependence for the Reynolds number of the changeover to the turbulent flow Re_{cr}, determined from the point of the minimum (extremum) of $\lambda_{hydr}/\lambda_{hydr.0}$ as a function N appears as [1]

$$Re_{cr} = 7.16\, Re_\omega^{0.78} + 2300\,. \tag{10}$$

From the data of [29]

$$Re_{cr} = 1.9\, Re_\omega^{0.9} + 2300\,, \quad 10^4 < Re_\omega < 5 \cdot 10^4\,. \tag{11}$$

The boundaries of the possible flow regimes are shown in Fig. 1 [1]. Curve 1 is constructed by (10). This curve is quite similar to curve 2 (11), which is obtained, like curves 5 and 6, in a much narrower range of Re and Re_ω numbers. Curves 3 and 4 determine the boundaries of the turbulent regime E and two partially suppressed regimes D_1 and D_2. Curves 5 and 6 determine the boundaries of the same regimes from the data of [29]. Curve 7 corresponds to the boundary of the transient regime B and the laminarized regime C. Curve 8, which is constructed from the data of [23, 35], corresponds to the boundary of laminarized flow. The disturbed laminar regime of flow is denoted by the letter A.

Laminar Flow.The axial velocity profiles in disturbed laminar flow that are obtained in [7] approach the turbulent type as Re and Re_ω increase (Fig. 2). The tangential velocity distribution is close to the profile in a forced vortex (law of rigid bodies) [7, 9]

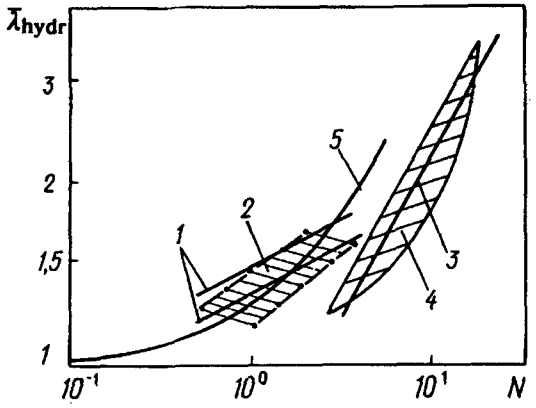

Fig. 3. Hydraulic resistance of axial rotating tube in disturbed laminar flow: 1) Eq. (12) for Re = 500 (lower curve) and 1000 (upper curve); 2) experiment [7] (the upper bound is Re = 1000, the lower is – 600); 3) Eq. (14); 4) experiment [23] (the upper bound is ωr_w = 5.32 m/sec, the lower bound is ωr_w = 1.33 m/sec; 5) Eq. (15).

$$u_\varphi / u_\omega = r / r_w .$$

The number Re has a slight effect on the distribution of the axial velocity [9]. In going from a fixed section to a rotating one, circular flow involves gradually new layers closer to the tube axis. For the rotation to establish completely according to the law of rigid bodies, about $255d$ for Re = 2300 are required, from the data of a pure theoretical calculation [36].

The data of [1, 7, 9, 23, 32, 37] demonstrate the increase in the hydraulic resistance of the disturbed laminar flow.

The experimental data of [7] are obtained in a channel with d = 5–20 mm, L/d = 200–388, Re = 600–1000, Re_ω = 600–2000, and N = 0.6–3.3 (the working fluid is water). These data agree well with the empirical expression [32]:

$$\bar{\lambda}_{hydr} = \frac{31}{64} Re_\omega^{0.16} , \tag{12}$$

where $\bar{\lambda}_{hydr} = \lambda_{hydr}/\lambda_{hydr.0}$, and $\lambda_{hydr.0}$ is determined by the Poiseuille formula

$$\lambda_{hydr.0} = 64/Re . \tag{13}$$

The experiments [23] are conducted in a channel with d = 0.0254 m, L/d = 68, Re = 300–2300, ωr_w = 0–5.23 m/sec, N = 2.5–17.5 (the working fluid is transformer oil) and are described by the equation

$$\bar{\lambda}_{hydr} = 0.65 N^{0.54} . \tag{14}$$

In [16], on the basis of the integral calculation method the following formula is obtained:

$$\bar{\lambda}_{hydr} = 1 + 0.25N . \tag{15}$$

As can be seen from Fig. 3 dependence (15) agrees satisfactorily with the data [7] for $N \leq 2.5$. In the region $N < 3.3$, the experimental results [23] are 20–35% lower than the data of [7]. For N = 3.3–17.5, there are only experimental data [23]. Apparently, for N = 3.3–4.3, $\bar{\lambda}_{hydr}$ can be determined to a relative degree of reliability as the arithmetical mean by formulas (12) and (14), while for $N > 4.3$, Eq. (14) should be employed.

As the number Re_ω increases the temperature profiles also approach the turbulent type [9] (Fig. 3).

A viscosity-gravitational regime of flow can develop in the presence of nonisothermicity. Rotation leads to transforming the two-vortex structure that is typical of this case to a one-vortex structure in the cross-section (a vortex that rotates in one direction with the tube wall increasing) for $N = N_1$ [9, 38]. However the center of the vortex remains above the tube axis. Motion becomes axisymmetric only once a certain value $N = N_2$ is attained [9, 38]. Analysis of the data of numerical calculations [9] enabled us to obtain the dependences for estimating N_1 and N_2 as a first approximation:

$$N_1 = 1.6\,\mathrm{Gr}/\mathrm{Re}^2, \quad N_2 = 20\,\mathrm{Gr}/\mathrm{Re}^2.$$

These expressions are obtained for $\mathrm{Re} \le 1000$, $N \le 1$, and $\mathrm{Gr}/\mathrm{Re}^2 \le 0.2$.

For flow when free convection has no effect on heat transfer, we approximated the numerical data of [9] on the segment of stabilized heat transfer by the equation

$$\mathrm{Nu}/\mathrm{Nu}_0 = (1 + 6.05 \cdot 10^{-4}\,\mathrm{Re}^{1.272} N)^{0.33}, \tag{16}$$

where $\mathrm{Re} = 200-2000$; $N = 0.25-20$; $\mathrm{Re}_\omega = 500-4000$, and $\mathrm{Nu}_0 = 4.36$. For sufficiently large values of Re and N, Eq. (16) appears as

$$\mathrm{Nu}/\mathrm{Nu}_0 = 0.0867\,\mathrm{Re}^{0.42} N^{0.33}. \tag{17}$$

The authors of [24] approximated their own experimental data for the heat-transfer coefficient averaged over the channel length in the viscosity-gravitational regime by the following expression:

$$\overline{\mathrm{Nu}}/\overline{\mathrm{Nu}}_0 = 1.75 N^{0.33} (\omega r_w/g)^{0.18}, \tag{18}$$

for $\mathrm{Re} = 2 \cdot 10^2 - 2 \cdot 10^3$; $\mathrm{Re}_\omega = (1.87-7.5) \cdot 10^4$; $\omega = 0-104.7$ 1/sec; $N = 7-500$; $\mathrm{Gr} = 5 \cdot 10^5 - 5 \cdot 10^7$; $d = 0.0317$ m; $L/d = 20.2$ (the working fluid is not indicated). The number $\overline{\mathrm{Nu}}_0$ was determined by M. A. Mikheev's formula [19]:

$$\overline{\mathrm{Nu}}_{0f} = 0.15\,\mathrm{Re}_f^{0.33}\mathrm{Pr}_f^{0.33} (\mathrm{Gr}\,\mathrm{Pr}_f)^{0.1} (\mathrm{Pr}_f/\mathrm{Pr}_w)^{0.25} \varepsilon_l. \tag{19}$$

Here the temperature difference in the Grashof number appears as $\Delta T = |T_w - T_{in}|$; the governing temperature is $T = (T_{in} + T_w)/2$; the characteristic dimension is d. The correction ε_l allows for a change in the number $\overline{\mathrm{Nu}}_{0f}$ along the tube length.

When deriving formula (19) it was assumed that the influence of the physical properties of the fluid, the temperature factor, and the length on heat transfer is the same as for a fixed tube.

In [16], using the integral calculation method the following relation

$$\mathrm{Nu}/\mathrm{Nu}_0 = (1 + 0.25N)^{0.33}, \tag{20}$$

is obtained, where

$$\mathrm{Nu}_0 = 1.39(d/L)^{1/3}\mathrm{Re}^{1/3}\mathrm{Pr}^{1/3}.$$

Expression (20) predicts very slight increases in the Nusselt number, which does not agree with the data of the experiment [24] and direct numerical modeling [9].

Formulas (16) and (17) agree satisfactorily with the experiments [24] for large Reynolds numbers Re = 1500–2000. In the region of small Re numbers, formula (16) predicts a relative increase in the number Nu that is by an order of magnitude smaller than that observed in the experiments [24]. Obviously under these conditions this is the result of the dominating influence of free convection. It seems impossible to directly compare formulas

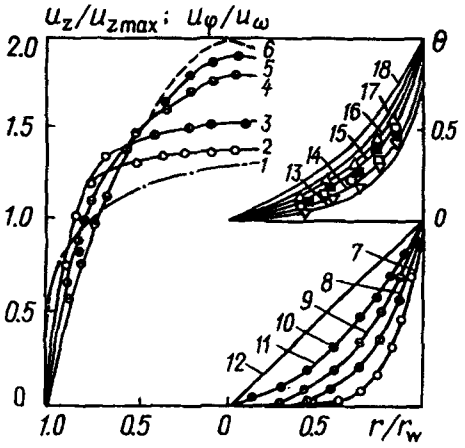

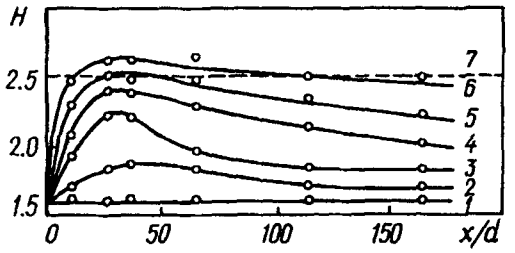

Fig. 4. Profiles of velocity (experiment [30], $N = 3$) and temperature (experiment and calculation [8], a stabilized segment) for turbulent flow in axial rotating tube and $Re = 10^4$: 1-6) $u_z/u_{z\,max}$; 7-12) u_φ/u_ω; 13-18) Θ; 1, 13) $N = 0$ (theory); 6) $N = 0$ (laminar flow, the theory); 2, 7) $z/d = 11$; 3, 8) 36; 4, 9) 68; 5, 10) 168; 11) $u_\varphi/u_\omega = (r/r_w)^2$; 12) $u_\varphi/u_\omega = r/r_w$; 14) $N = 0.5$; 15) 1; 16) 2; 17) 3; 18) 5.

Fig. 5. Change in form factor H along tube [30] ($Re = 10^4$): 1) $N = 0$; 2) 0.5; 3) 1; 4) 2; 5) 3; 6) 4; 7) $H = 2.5$, laminar flow for $N = 0$.

(16) and (18) since neither the type of the working fluid nor its properties are indicated in [24]. The coincidence of the values of the indexes on the number N in formulas (15)-(18) and (20) is noteworthy, too.

Turbulent Flow. Using visualization the authors of [30] revealed a certain sequence of the development of turbulent flow in a rotating tube when the fluid enters from a pre-embedded fixed segment.

In the case of moderate rotation ($Re = 10^4$, $N = 1$) on the initial segment with $z/d = 12-28$ there is a laminarized boundary layer near the wall and a nonrotating turbulent core. In the cross-sections with $z/d = 36-52$ and further, the turbulence of the core generates turbulence "spots" in the laminarized layer. In the cross-sections with $z/d = 94-110$, the rotation involves axial layers of the tube, and the turbulent "spots" observed earlier are uniformly diffused along the flow radius. Next the turbulence "spots" appear periodically again and no flow laminarization is observed, the axial velocity profiles differing (towards laminarization) from the usual turbulent cross-section. In strong rotation ($Re = 10^4$, $N = 3$) on the length $z/d = 12-52$ flow in the rotating layer becomes completely laminar despite a single "spot" of turbulence. On the segment with $z/d = 94-110$, the laminar rotating flow involves the entire cross-section of the tube, and the frequency of appearance of turbulence "spots" is very low. On the segment $z/d = 170-180$, the rotation destabilizes the flow again; turbulence in the flow and the "spot" frequency increase somewhat.

For $N = 5$ on the segment with $z/d = 94-110$ the flow occurs intermittently in time: with an interval of 0.6 sec there follows laminarization, the beginning of instability, the appearance of turbulent "spots," and relaminarization. On this basis the authors of [40] relate the bursts of turbulence to vortex decomposition in the flow.

The described character of the development of flow for $N = 3$ corresponds to the axial velocity profiles (Fig. 4). In the initial cross-sections in the wall region, the profiles have a laminarized form, while in the region of the nonrotating turbulent core u_z is practically constant. Away from the inlet to the tube the velocity profiles already acquire a typical laminarized form in the entire cross-section. The axial velocity profiles in [30] are also constructed in the coordinates $(r_w - r)/\delta^{**}$, i.e., in a larger scale. Even the same, in practice (in the coordinates r/r_w), distributions u_z away from the inlet to the tube turn out to be sensitive to local changes in the degree of turbulence, deviating towards turbulization or laminarization.

The change in the profile of the rotational velocity along the tube length is shown in Fig. 4 [30]. Regardless of N the distribution of the circular velocity for steady-state flow follows the law [7-11]

$$u_\varphi/u_\omega = (r/r_w)^2. \tag{21}$$

The development of the flow along the tube is clearly characterized by the form factor H, which is calculated by ordinary formulas for the axial velocity [30] (Fig. 5). For laminar flow in a fixed tube, $H = 2.5-2.6$. The laminarizing effect of rotation induces a "jump" in H at the inlet to the tube, the more pronounced, the higher N (when $N \geq 3$ $H \geq 2.5$). The form factor H attains its maximum for $z/d \approx 30$ and then decreases asymptotically to an approximately constant N-dependent value, which demonstrates enhancement of turbulence.

The substantial attenuation of turbulence and its renewed buildup along the tube length are also demonstrated by the distributions of the pulsation $(\overline{u'_\varphi}^2/u^2_{z\,\text{inl}})^{1/2}$ [30]. Detailed measurements of turbulent characteristics, including those at the moment of the "bursts," are presented in [31].

The successive development of velocity profiles from a turbulent profile to laminarized ones in the region of steady-state (completely rotating) flow for different N and Re = idem is presented in [7, 9-11]. These distributions, obtained in experiments and calculations, are similar to the u_z profiles in Fig. 4, the curves passing increasingly higher as N increases.

The authors of [11] solved Eq. (3) with allowance made for the above-described simplifications for the region of steady-state flow, employing the mixing length model (6)-(8), in which l_0 was determined by the known Nikuradze formula with the Van Drist damping cofactor

$$\bar{l}_0 = (0.14 - 0.08\bar{r}^2 - 0.06\bar{r}^4)\,[1 - \exp(-y^+/26)].$$

The tangential velocity was described by expression (21). It was established that the effect of rotation on the axial velocity profile is characterized by the parameter z (formula (9)), the expression for the universal distribution u_z^+ appearing as

$$u_z^+ = u_{zb}^+ f + u_{zc}^+ (1 - f), \tag{22}$$

where u_{zb}^+ and u_{zc}^+ are the velocity distributions in the wall region and in the flow's core, respectively.

$$u_{zb}^+ = \frac{1}{\kappa_1}\ln(1 + \kappa_1 y^+) + 7.8\left[(1 - \exp(-y^+/y_1^+))\frac{\mathrm{Re}_\tau}{\mathrm{Re}_{\tau 0}} - \frac{y^+}{y_1^+}\exp(-by^+)\right]; \tag{23}$$

$$u_{zc}^+ = u_{z\max}/u_\tau - A\bar{r}^B. \tag{24}$$

Here

$$\kappa_1 = 0.4\frac{\mathrm{Re}_\tau}{\mathrm{Re}_{\tau 0}}\left[\left(\frac{Z}{\mathrm{Re}_\tau}\right)^2 + 1\right]^{-3.5};$$

$$y_1^+ = 11\frac{\mathrm{Re}_\tau}{\mathrm{Re}_{\tau 0}};\quad b = 0.33\left\{\frac{\mathrm{Re}_\tau}{\mathrm{Re}_{\tau 0}}\left[\left(\frac{Z}{\mathrm{Re}_\tau}\right)^2 + 1\right]^{-3.5}\right\}^{1/2};$$

$$A = (0.06052Z^2 + 5.4Z + 25.705)^{1/2};$$

$$B = 1.55 + 0.338\,[1 - \exp(-0.0553Z)];$$

$$f = \exp(-a_1(1 - \bar{r}));\quad a_1 = 5\,\mathrm{Re}_{\tau 0}/\mathrm{Re}_\tau;$$

$\mathrm{Re}_{\tau 0} = u_{\tau 0} r_w/\nu$ and $u_{\tau 0}$ is calculated for a fixed tube. On the basis of the Blasius formula for the hydraulic resistance in turbulent flow in a fixed tube

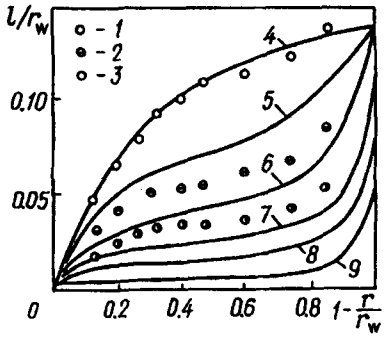

Fig. 6. Distribution of mixing length for turbulent flow in axial rotating tube on segment of stabilized flow ($Re = 2 \cdot 10^4$). The experiment [7]: 1) $N = 0$; 2) 0.5; 3) 1.0; calculation for $\beta = 0.4$ [7]; 4) $N = 0$; 5) 0.5; 6) 1.0; 7) 1.5; 8) 2.0; 9) 3.0.

$$\lambda_{hydr.0} = 0.316\,Re^{-0.25}, \tag{25}$$

the expression for the Reynolds number $Re_{\tau 0}$ appears as

$$Re_{\tau 0} = (0.3164/32)^{1/2} Re^{0.875}.$$

The maximum-to-average velocity ratio $u_{z\,max}/u_{z\,av}$ in [7] increased linearly from ≈ 1.3 to 2 (this value is characteristic of laminar flow) in the range $0 < N < 3.5$, the number Re having no effect on this ratio. The relationship $u_{z\,max}/u_{z\,av}$ derived in [8] shows a weaker effect of rotation. Thus, for $N = 5$ in [8], $u_{z\,max}/u_{z\,av}$, and a magnitude equal to two is attained asymptotically when $N \geq 10$.

In [11], from the same premises that led to formulas (22)-(24), the following relationship is derived:

$$\frac{u_{zmax}}{u_\tau} = \frac{Re}{2\,Re_\tau} + \frac{2A}{B+2},$$

where A and B are found above. The data of [8] and [11] practically coincide. Distributions of the mixing length $\bar{l}$ in the steady-state flow region have the form

$$\bar{l} = \bar{l}_0 \left(\frac{du_z^+}{dy^+}\right)^4 \Bigg/ \left[\left(\frac{du_z^+}{dy^+}\right)^2 + \left(1 - \frac{y^+}{Re_\tau}\right)^2 \left(\frac{Z}{Re_\tau}\right)^2\right]^2,$$

where the universal velocity u_z^+ is determined by formulas (22)-(24).

Figure 6 shows the distributions of the function l in this region for different values of N [7], which demonstrate the conservative effect of rotation on originally turbulent flow.

In [3, 24], it is shown that the rotation alters the spectrum of turbulent pulsation frequencies: the amplitudes maximum shifts to a high-frequency region. This confirms the hypothesis that the mass forces suppress primarily low-frequency large-scale pulsations.

An overall reduction of the turbulence level leads to a decrease in the tangential stress $\tau_{\varphi w}$. In [29], an expression is obtained that approximates experimental data for $N < 0.9$:

$$2\tau_{\varphi w}/(\rho u_{zmax}^2 N) = 0.00317 \exp\,[-0.023\,(L/d)].$$

For larger values of N, greater suppression of turbulence and a stronger decrease in $\tau_{\varphi w}$ were observed.

The stabilizing effect of rotation on the flow leads to a decrease in the hydraulic resistance of the rotating segment (Fig. 7). In relative form, $\bar{\lambda}_{hydr} = \lambda_{hydr}/\lambda_{hydr.0}$, where $\lambda_{hydr.0}$ is determined by the Blasius formula (25).

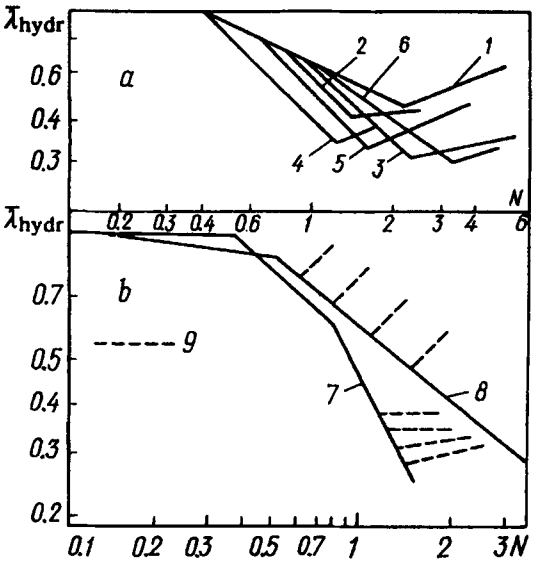

Fig. 7. Hydraulic resistance of axial rotating tube in turbulent flow: 1-7) experiment [29]; 1) $L/d = 30$, $\mathrm{Re} = 10^4$; 2) 50 and $3.5 \cdot 10^4$; 3) 50 and $5.5 \cdot 10^4$; 4) 70 and $2 \cdot 10^4$; 5) 70 and $3.5 \cdot 10^4$; 6) 70 and $7.5 \cdot 10^4$; 7) $L/d \geq 100$, Eqs. (28) and (29); 8) $L/d \geq 100$, Eqs. (26) and (27); 9) $L/d \geq 100$, transition to laminar flow.

For small rotational velocities $\bar{\lambda}_{hydr}$ first remains equal to unity (turbulent flow) and then decreases and attains a minumum. A sharp increase in $\bar{\lambda}_{hydr}$ thereafter for ω = idem and $\mathrm{Re} = \mathrm{Re}_{cr}$ as N increases demonstrates the transition to a laminar flow regime. For small tube lengths $L/d < 70$, the data [29] have a large spread (Fig. 7a); however, when $L/d \geq 100$ this spread is small and $\bar{\lambda}_{hydr}$ is almost independent of the tube length.

For $L/d \geq 100$, it was found in [29] for

$$N < 0.35\,, \quad \bar{\lambda}_{hydr} = 1\,;$$

$$0.35 \leq N \leq 0.8\,, \quad \bar{\lambda}_{hydr} = 0.579 N^{-0.52}\,; \tag{26}$$

$$0.8 \leq N \leq 1.2\,, \quad \bar{\lambda}_{hydr} = 0.47 N^{-1.42}\,. \tag{27}$$

Based on earlier experimental data [40, 41] V. K. Shchukin [1] presented the following relations (Fig. 7b):

$$N < 0.125\,, \quad \bar{\lambda}_{hydr} = 1\,;$$

$$0.125 \leq N \leq 0.475\,, \quad \bar{\lambda}_{hydr} = 0.89\,(2N)^{-0.086}\,; \tag{28}$$

$$0.475 \leq N \leq 5\,, \quad \bar{\lambda}_{hydr} = 0.865\,(2N)^{-0.535} \tag{29}$$

whicht serve as the upper bound of the results [29].

In [16], the equation (obtained by a calculation method)

$$\bar{\lambda}_{hydr} = 200\,\mathrm{Re}^{-0.75}\,[1 + 0.25N + (0.005\,\mathrm{Re}^{0.75} - 0.0002\,\mathrm{Re}_{\omega} N - 1)] \tag{30}$$

TABLE 1. Eigenvalues λ_n^2 and Constants B_nH_n (1) for Different Values of Re Number and Parameter Δ in Formula (32) [10]

Re	Δ	N	λ_1^2	λ_2^2	λ_3^2	λ_4^2	λ_5^2	B_1H_1 (1)	B_2H_2 (1)	B_3H_3 (1)	B_4H_4 (1)	B_5H_5 (1)
10,000	0.5	0.0	0.969	281.4	806.8	1559	2550	0.969	0.007	0.0041	0.0029	0.0022
		1.0	0.959	132.1	412.8	829.4	1379	0.959	0.0113	0.0050	0.0033	0.0025
		5.0	0.866	23.72	73.52	149.7	252.3	0.864	0.0508	0.0199	0.0112	0.0074
		20.0	0.809	14.03	43.34	88.68	150	0.803	0.0771	0.0299	0.0164	0.0105
10,000	2	0.0	3.55	286.9	816.2	1572	2566	0.887	0.0238	0.0144	0.0105	0.0079
		1.0	3.41	136.3	419.6	837.1	1389	0.853	0.0374	0.0172	0.0116	0.0088
		5.0	2.44	26.7	77.32	154.2	257.4	0.595	0.1202	0.0562	0.0342	0.0236
		20.0	2.00	16.51	46.55	92.42	154.2	0.477	0.1487	0.0746	0.0459	0.0315
10,000	10	0.0	12.18	306.9	851.9	1624	2633	0.606	0.0590	0.0394	0.0315	0.0256
		1.0	10.67	150.6	439.6	866.4	1427	0.526	0.0829	0.0435	0.0315	0.0266
		5.0	4.55	32.58	86.46	166.3	272.2	0.207	0.1000	0.0661	0.0497	0.0397
		20.0	3.17	20.27	52.76	100.9	164.7	0.138	0.0843	0.0622	0.0493	0.0406
50,000	0.5	0.0	0.99	1117	3285	6432	10,550	0.991	0.0017	0.0009	0.0006	0.0005
		1.0	0.986	437.8	1399	2848	4778	0.987	0.0033	0.0013	0.0008	0.0006
		5.0	0.925	45.5	144.3	295.8	499.8	0.924	0.0285	0.0106	0.0058	0.0038
		20.0	0.809	14.09	43.52	89	150.6	0.804	0.0768	0.0298	0.0163	0.0105
50,000	2	0.0	3.854	1123	3293	6445	10,563	0.964	0.0064	0.0034	0.0025	0.002
		1.0	3.794	442	1404	2855	4787	0.949	0.0125	0.005	0.0031	0.0023
		5.0	3.004	49	148.5	300.6	505.2	0.745	0.0855	0.0349	0.0200	0.0134
		20.0	2.004	16.58	46.73	92.77	154.8	0.478	0.1484	0.0745	0.0458	0.0315
50,000	10	0.0	16.81	1148	3334	6503	10,641	0.84	0.0249	0.0136	0.0101	0.0084
		1.0	15.71	461.4	1429	2887	4826	0.784	0.0460	0.0193	0.0121	0.0091
		5.0	7.282	59.17	162.5	317.9	525.3	0.343	0.1256	0.0704	0.0471	0.0347
		20.0	3.179	20.35	52.98	101.3	165.3	0.138	0.0843	0.0621	0.0493	0.0406

is presented. It is applicable for positive values of the expression in the parentheses, i.e., when $N \leq [(25\mathrm{Re}^{0.75} - 5000)/\mathrm{Re}]^{1/2}$. As Re increases from 5000 to 50,000 the limiting value of N decreases from 1.4 to 1.25. Depending on the number Re the values of $\bar{\lambda}_{\mathrm{hydr}}$ that are calculated by formula (30) can be 30–40% lower than the experimental data [29, 40, 41].

In the region of laminarized flow, the hydraulic resistance is higher than in laminar flow in the fixed tube, and it decreases as N increases (when $\mathrm{Re} < \mathrm{Re}_{cr}$). This demonstrates the preservation in the flow of the remnants of turbulence, which is transferred mainly by a longitudinal pulsation, which is maximal and not directly affected by radial rotation [1, 25]. For this case in [1] the expression

$$\bar{\lambda}_{hydr} = \lambda_{hydr}/\lambda_{hydr.0} = 3.2N^{-0.44},$$

is obtained, which holds for $\mathrm{Re}_\omega = 2.8\cdot 10^2 - 2.2\cdot 10^3$ and $\mathrm{Re} < \mathrm{Re}_{cr}$. Here $\lambda_{hydr.0}$ is calculated by relation (13).

Experimental data [8] for hydrodynamically and thermally steady flow demonstrate profiles of the temperature Θ approaching the laminar type (Fig. 4), which is in agreement with the overall picture of turbulence suppression in the tube.

The decrease in the pulsations $\overline{u'_\varphi T'}$ and $\overline{u'_r T'}$ as a result of the conservative effect of rotation is demonstrated by the computational data of [6].

Experimental and computational data on heat transfer are given in [8, 10, 27, 35]. They show that rotation reduces substantially the Nusselt number. Thus, for $\mathrm{Re} = 5000$ and $N = 5$, the ratio $\mathrm{Nu}/\mathrm{Nu}_0 \approx 0.37$ [8].

The only known empirical similarity equation was obtained in [27] as a result of processing of experimental data for the initial segment of a heated tube with $d = 97.6$ mm, $L = 3000$ mm, $\mathrm{Re} = (0.3-3)\cdot 10^5$, $N = 0-0.8$, $\omega = 0-122.52$ sec^{-1} (the working medium is air). To calculate the local Nu and average $\overline{\mathrm{Nu}}$ Nusselt numbers, the authors of [27] recommended the following dependences:

$$\mathrm{Nu}/\mathrm{Nu}_0 = 1 - \mathrm{th}\left[1 + 0.001335\frac{\mathrm{Re}_\omega}{\mathrm{Re}^{7/8}} - \exp\left(-0.23\frac{\mathrm{Re}_\omega}{\mathrm{Re}^{7/8}}\right)\right];$$

$$\overline{\mathrm{Nu}}/\overline{\mathrm{Nu}}_0 = 1 - \mathrm{th}\left[1 + 0.000175\frac{\mathrm{Re}_\omega}{\mathrm{Re}^{0.685}} - \exp\left(-0.03\frac{\mathrm{Re}_\omega}{\mathrm{Re}^{0.685}}\right)\right], \quad (31)$$

where

$$\mathrm{Nu} = 0.022\,\mathrm{Re}_z^{0.8}\,\mathrm{Pr}_z^{0.43}\,1.38\,(z/d)^{-0.12};$$

$$\overline{\mathrm{Nu}} = 0.021\,\mathrm{Re}^{0.8}\,\mathrm{Pr}^{0.43}\,\varepsilon_l.$$

Here the numbers Re_z and Pr_z are found for the local cross-sections of the channel; ε_l is a correction for the length of the initial segment.

The experiments of [8] were conducted in a tube with $d = 50$ mm, $L/d = 120$, $\mathrm{Re} = (0.5-5)\cdot 10^4$, $\mathrm{Re}_\omega = 0-25{,}000$, $\omega = 0-314.2$ sec^{-1}, $N = 0-5$ (the working medium is air). For $\mathrm{Re} = 5000$ and $N = 3-5$, the experimental data [8] for $\mathrm{Nu}/\mathrm{Nu}_0$ are 20–25% higher than those calculated by formula (31). For smaller values of N, a better agreement is observed.

In [8, 10], the authors obtained analytical solutions of the problem using approximation (21) that describe sufficiently well the experimental data of [8]. The expression of [10] for the local Nusselt number appears as

$$\mathrm{Nu} = \left[2\Delta\sum_{n=1}^{\infty} B_n H_n(1)\exp\left(-\lambda_n^2\bar{z}\right)\right]\times$$

$$\times\left[1 - 2\Delta\sum_{n=1}^{\infty}\frac{B_n H_n(1)}{\lambda_n^2} - \sum_{n=1}^{\infty} B_n H_n(1)\exp\left(-\lambda_n^2\bar{z}\right)\right], \quad (32)$$

where $\bar{z} = 4z/(d\mathrm{RePr})$; $\Delta = kr_w/\lambda$; k is the heat-transfer coefficient, which is determined by the relation

$$\frac{1}{k} = \frac{r_w}{\alpha_0 r_0} + \frac{r_w}{\lambda_w} \ln\left(\frac{r_w}{r_0}\right),$$

in which α_0 and r_0 are the coefficient of heat transfer on the exterior wall of the tube and its outside radius, λ_w is the heat-transfer coefficient for the tube material. The magnitude (1) of the argument of the function B_nH_n corresponds to the value of the dimensionless radius r/r_w. The coefficients B_nH_n (1) and λ_n^2 for the first five terms of the series are given in [10] as a table (here it is abridged). Expression (32) indicates a substantial increase in the length of the initial thermal segment as the rotation parameter$B$ increases as well as independence of the obtained results of the form of the "thermal" boundary conditions on the wall.

In [16], a dependence is proposed that is obtained on the basis of an integral calculation method:

$$\overline{Nu} = 1.39\,(Re\,Pr\,d/L)^{1/3}\,[1 + 0.25N + [0.005\,Re^{0.75} - 0.0002\,Re_\omega\,N - 1)]^{1/3}.$$

It can be used for positive values of the expression in the parentheses (see comments on formula (30)). The resultant relative values of the Nusselt number $\overline{Nu}/\overline{Nu}_0$ are understimated by 20–40% as compared to the data of [8, 27] and Eqs. (31) and (32).

2. Influence of Various Factors. In [42-45], the authors investigated the influence on the turbulent flow in a tube of the initial swirl, which is different from the swirl on the main segment. In [45], the development of a recirculation zone and return flow near the axis was observed.

A special case is the localized segment of the reconstruction of an undeveloped (rectangular) velocity profile at the inlet to the tube [3]. Here, a "burst" of turbulence is observed which is due to a strong shear caused by the rotation of the wall [3].

The axial velocity profiles on this segment (z/d = 2.7–28.5) are the same (in the coordinates $(r_w - r)/\delta_z^{**}$) and lie between the standard distribution for laminar and turbulent flows.

For the circular velocity profile, the expression $1 - u_\varphi/u_\omega = [(r_w - r)/(10\delta_{z\varphi}^{**}]^{0.3}$ is obtained in [3]. The distributions of the momentum thicknesses determined by the equations

$$\delta_z^{**} = \int_{r_w-\delta}^{r_w} \frac{u_z}{u_{z\,inl}}\left(1 - \frac{u_z}{u_{z\,inl}}\right)\frac{r}{r_w}\,dr,\quad \delta_{z\varphi}^{**} = \int_{r_w-\delta}^{r_w} \frac{u_z}{u_{z\,inl}}\,\frac{u_\varphi}{u_\omega}\left(\frac{r}{r_w}\right)^2 dr,$$

become flat as N increases, which reflects the retardation of the development of the boundary layer due to rotation [3].

In the cross-section z/d = 2.7, the circular component of the pulsations $(\overline{u_\varphi'^2})^{1/2}/u_{z\,inl}$ increases by a factor of 2–3 for practically constant components $(\overline{u_z'^2})^{1/2}/u_{z\,inl}$ and $(\overline{u_r'^2})^{1/2}/\overline{u_z}_{inl}$. The tangential stresses $\overline{u_z'u_\varphi'}/u_{z\,inl}^2$ and $\overline{u_r'u_\varphi'}/u_{z\,inl}^2$ increase by a factor of 1.5–2, too, while the component $\overline{u_z'u_r'}/u_{z\,inl}^2$ remains practically constant. The increase in the indicated Reynolds stresses is due to the presence of strong shear that is the most pronounced in this zone of the tube.

In the cross-section z/d = 28.5, all the pulsation components decrease, $(\overline{u_z'^2})^{1/2}/u_{z\,inl}$ and $(\overline{u_\varphi'^2})^{1/2}/u_{z\,inl}$ becoming noticeably smaller in the wall region $(r_w - r)/\delta_z^{**} \le 1$) and $(\overline{u_z'^2})^{1/2}/u_{z\,inl}$ being uniform in the entire boundary layer. The stress $\overline{u_z'u_z'}/u_{z\,inl}^2$ is affected rather substantially by the rotation, decreasing as N increases. The turbulent stresses $\overline{u_z'u_\varphi'}/u_{z\,inl}^2$ and $\overline{u_r'u_\varphi'}/u_{z\,inl}^2$, as in the case of a fixed tube, are small in magnitude.

The total energy of turbulence

$$q^2/u_{z\,inl}^2 = (\overline{u_z'^2} + \overline{u_r'^2} + \overline{u_\varphi'^2})/u_{zmax}^2$$

in the cross-section z/d = 2.7 [3] increases as N increases, which reflects the destabilizing effect of rotation. In the cross-section z/d = 9.7, all the distributions of the turbulence energy for N = 0–0.83 merge into one line, since the stabilizing and destabiling effects are balanced. In far cross-sections when the flow is steady-state q^2 decreases noticeably, which demonstrates the predominance of the stabilizing effect.

The influence of injection and rotation on the parameters of turbulent flow is qualitatively similar [2, 46]. Although, in strong injection, the velocity u_z can increase somewhat near the wall and $u_{z\,max}$ can decrease because of the considerable induced negative pressure gradient. The temperature profiles Θ are characterized by a particularly noticeable extension on the axis and displacement from the wall.

The influences of rotation and suction are opposite, and the final result depends on the relation of these factors [2]. As the suction intensity and N increase the velocity maximum shifts to the wall, the temperature profile approaches rod-shaped, and the hydraulic resistance and the number Nu increase.

Rotation can have both a destabilizing effect and a stabilizing one on the flow of a thin water jet in a tube through which the air is pumped [47, 48].

With the beginning of rotation, a portion of the fluid in the form of a film is entrained by the tube wall and the remaining fluid changes to a "bead" along the lower generatrix of the tube. As the rotational velocity increases the "bead" decomposes into cells 2–3 calibers long. Then in the middle of the cells there form fluid rings to the point of the formation of a continuous annular film with toroidal vortices at regular intervals on its surface. For large revolutions, the disturbed character of the flow is suppressed, the film becomes transparent, and its surface becomes smooth. When the tube is rapidly stopped the rotational flow (that continues under its own momentum) becomes vortical again, and the efflux of the fluid from the open end of the channel becomes pulsating [47].

The determining role in the generation of the described toroidal vortices (the Taylor–Görtler type) is played by the difference in the tube and film velocities. The lag of the liquid that appears with the beginning of the rotation becomes maximal at some moment and then disappears gradually.

A more complex character of the change and interaction of these toroidal vortices was observed in [48].

The experimental data [47] for the Taylor number $\mathrm{Ta} = (\Delta u_\varphi \delta/\nu_{fl})\sqrt{\delta/r_w}$ (where Δu_φ is the difference between the tangential velocity of the flow and that of the wall channel; δ is the thickness of the fluid film) are described with an error of up to 18% by the dependence with the maximum

$$\mathrm{Ta} = 1.6\,(G_{fl}/G_{fl\,max})\,(\omega^2 r_w/q)^2 \exp\,[-0.4\,(\omega^2 r_w/g)]$$

for the flow rate of the fluid G_{fl} from 0 to $G_{fl.max} = 0.13$ m^3/h, Ta = 0–32, $\omega^2 r_w/g = 0$–20, $\delta/r_w = 0$–0.1. The film thickness was determined by the formula

$$\delta = [G_{fl}^2/(4\pi^2 r_w^3 \omega_{film}^2)]^{1/3},$$

where ω_{film} is the angular rotational velocity for the film. However, in [47], no minimum critical value of Ta is determined for which vortices develop.

For the heat transfer from the fluid to the wall, the authors of [47] derived the extremal dependence

$$\mathrm{Nu}/\mathrm{Nu}_0 = 1 + 1.8\,(G_{fl}/G_{fl\,max})^{0.2}\,(\omega^2 r_w/g)\exp\,(-0.07\omega^2 r_w/g),$$

which describes, with an error of up to 30%, the flow for $d = 0.04$ m, $L/d = 10$, $0 \le \omega^2 r_w/g \le 60$, $0.004 \le G_{fl} \le 0.15$ m^3/h (or $\mathrm{Re}_{fl} = 50$–6500). In [48], it is shown that the heat transfer in a tube partially filled with a liquid proceeds with the same intensity as in an entirely filled one. This is attributable to the fact that during rotation the unfilled portion of the tube is covered with a film of the liquid (a thickness of 0.5 mm), which receives heat from the wall and then mixes with the remaining liquid.

3. Other Types of Channels. In [48], experimental and computational data are given for an axial rotating tube that is closed at one end. In this channel, under the a action of the radial pressure drop generated by centrifugal forces, there develops combined flow with longitudinal rod suction of the air near the tube axis and annular peripheral back flow of the air to the atmosphere. A special feature of the laminar flow of a fluid in a vertical rotating tube with a rectangular profile of axial velocity u_z at the inlet is the possibility of the wall return flows of the fluid occurring [50]. As a result of a theoretical analysis it was found in [50] that for $\omega^2 < 5.77$ the

profile of the axial velocity u_z at the inlet corresponds to Poiseuille flow; for $5.77 \leq \omega^2 \leq 25.91$, the flow of the fluid near the wall slows down, and the profile of the velocity u_z is deformed. When $\omega^2 > 25.91$ wall return flows occur at some distance from the inlet to the tube (to determine which, a rather complex expression is given in [50]).

Rotation that destabilizes laminar flow can lead to the occurrence of periodic pulsations of the flow velocity that are attenuated along the length even in a straight tube, which is most clearly observed in the experiments [51] for $Re_{inl} = 550$ and $1/N = 0.31$. The change in cross-sectional area investigated in [51] (the apex angle is $\pm 1.87^\circ$) has a negligible effect on the stability of the developing wave process. In a divergent tube, the amplitude of oscillating disturbances is smaller than in a convergent tube. However, in the first case, the overall retardation of the flow together with decreasing pulsation lead to the occurrence of return flow and opposite rotation in the vicinity of the axis of the tube at its inlet. The formation and decomposition of a toroidal vortex at this site are also confirmed by flow visualization.

The described mechanism as the authors of [51] think, can take place in the case of vortex decomposition in a swirling flow in a fixed divergent tube, too.

Conclusions. The rotation of channels about their axis has a substantial effect on the character of flow in them and the intensity of transfer processes. In channels of a constant cross-section, the rotation disturbs and turbulizes the originally laminar flow. The hydraulic resistance and the Nusselt number in this case can increase by a factor of 3–5. Conversely, the originally turbulent flow becomes laminarized while the Nusselt number and the coefficient of hydraulic resistance can decrease by 60–70%.

The conditions at the inlet to the channel have a substantial effect on the character of the flow. Thus, the supply of a fluid with a rectangular profile of axial velocity in turbulent flow has an additional turbulizing effect on the flow in the initial cross-sections of the channel.

A change in the geometry of the channel or its disposition can fundamentally alter the character of the flow. Return currents occur in a vertical channel while velocity pulsations, return flow near the axis, and vortex decomposition occur in a divergent one.

The intensity of tube rotation is the governing factor that determines the flow structure for the flow of a fluid that does not fully occupy the cross-section of the channel. Analysis is given for different vortex flows that occur in this case as well as of the influence of injection, suction, and flow in a tube that is closed at one end.

NOTATION

r, φ, z, cylindrical coordinates; u_r, u_φ, u_z, radial, circular (tangential), and axial components of the flow velocity; F_r, F_φ, F_z, components of mass forces acting in fluid; T, temperature; p, static pressure; t, time; μ, ν, coefficients of dynamic and kinetic viscosity; ν_t, turbulent viscosity; ρ, density; λ, thermal conductivity; C_p, heat capacity; $u_{z\,av}$, velocity averaged over cross-section; β_{exp}, coefficient of thermal expansion; g, free fall acceleration; $Gr = g\beta_{exp}\Delta T d^3/\nu^2$, Grashof number; d, r_w, diameter and radius of tube; ω, angular rotational velocity; $u_\omega = \omega r_w$, circular velocity on wall; $\Theta = (T - T_w)/(T_{max} - T_w)$; T_{max}, temperature on tube axis; $Re = u_{z\,av}d/\nu$, Reynolds axial flow number; $Re_\omega = u_\omega d/\nu$, Reynolds rotational number; $Re_\tau = u_\tau r_w/\nu$; $u_\tau = [(\tau_{rz})_w/\rho]^{1/2}$, dynamic velocity; l, mixing length; $\bar{l} = l/r_w$; L, channel length; λ_{hydr}, hydraulic resistance of channel; $\overline{Nu} = \bar{\alpha}d/\lambda$, average Nusselt number; $\bar{\alpha}$, average heat-transfer coefficient; $Pr = \nu/a$, Prandtl number; a, thermal diffusivity; $u_z^+ = u_z/u_\tau$, universal velocity; $y^+ = u_\tau(r_w - r)/\nu$, universal coordinate; $\bar{r} = r/r_w$; $u_{z\,max}$, velocity on channel axis; δ^{**}, momentum thickness; δ, boundary layer thickness; G_{fl}, mass flow-rate of fluid through channel; the symbols "$\bar{\ }$" signify time-averaged pulsation characteristics. Subscripts and superscripts: w and f, conditions on the wall and the flow core; 0, flow in fixed tube; inl, condition at inlet to channel; fl, fluid in two-phase flows.

REFERENCES

1. V. K. Shchukin, Heat Transfer and Hydrodynamics of Internal Flows in Fields of Mass Forces [in Russian], Moscow (1980).

2. V. M. Eroshenko, L. I. Zaichik, and I. A. Ten, Improving the Efficiency of Processes in Heat Engines [in Russian], Moscow (1985), pp. 20-28.
3. K. Kikuyama, M. Murakami, and K. Nishibori, Trans. ASME, J. Fluids Engng., 105, No. 2, 154-161 (1983).
4. B. S. Tursunov, Rheology of Turbulent Flows [in Russian], Leningrad (1989), pp. 25-40.
5. S. Hirai, T. Takagi, and M. Matsumoto, Trans. ASME, J. Fluids Engng, 110, No. 7, 424-431 (1988).
6. S. Hirai and T. Takagi, JSME Int. J., Ser. II, 31, No. 4, 694-700 (1988).
7. K. Kikuyama, M. Murakami, K. Nishibori, and K. Maeda, Bull. JSME, 26, No. 214, 506-513 (1983).
8. G. Reich and H. Beer, Int. J. Heat Mass Transfer, 32, No. 3, 551-562 (1989).
9. G. Reich, B. Weigand, and H. Beer, Int. J. Heat Mass Transfer, 32, No. 3, 563-574 (1989).
10. B. Weigand and H. Beer, Int. J. Heat Mass Transfer, 35, No. 7, 1803-1809 (1992).
11. B. Weigand and H. Beer, Appl. Sci. Res., 52, No. 2, 115-132 (1994).
12. E. P. Sukhovich, Izv. Akad. Nauk Latv. SSR, Ser. Fiz. Tekhn. Nauk, No. 5, 8-87 (1985).
13. B. E. Launder, C. H. Priddin, and B. I. Sharma, Trans. ASME, J. Fluids Engng, 99, No. 1, 231-239 (1977).
14. H. Kawamura and T. Michima, Trans. JSME, Ser. B, 57, No. 536, 1251-1256 (1991).
15. P. Bradshaw, J. Fluid Mech., 36, 177-191 (1969).
16. I. I. Alekseev, G. A. Vitkov, L. P. Kholpanov, and S. N. Sherstnev, Zh. Prikl. Khim., 6, No. 2, 327-330 (1989).
17. S. Ya. Gertsenshtein and N. V. Nikitin, Izv. Akad. Nauk SSSR, Mekh. Zhidk. Gaza, No. 4, 22-28 (1985).
18. P. A. Mackrodt, J. Fluid Mech., 73, 153-164 (1976).
19. H. H. Nagib, S. Lavan, A. A. Fejer, and L. Wolf, Phys. Fluids, 14, 760-768.
20. K. Nishibori, K. Kikuyama, and S. Yoshioka, Trans. JSME, Ser. B, 57, No. 538, 1941-1946 (1991).
21. T. J. Pedley, J. Fluid Mech., 35, 97-115 (1969).
22. N. Toplosky and T. R. Akylas, J. Fluid Mech., 190, 39-54 (1988).
23. A. I. Borisenko, O. N. Kostikov, and V. I. Chumachenko, Samolyotostroenie Tekhnika, Vozdushnogo Flota (Aircraft Industry and Air Force Engineering), Kharkov, Issue 32, 42-45 (1973).
24. A. I. Borisenko, O. N. Kostikov, and V. I. Chumachenko, Aerodinamika Teploperedacha Elektricheskikh Mashinakh (Aerodynamics and Heat Transfer in Electric Motors), Kharkov, Issue 4, 63-71 (1974).
25. A. I. Borisenko, O. N. Kostikov, and V. I. Chumachenko, Samolyotostroenie Tekhnika Vozdushnogo Flota (Aircraft Industry and Air Force Engineering), Issue 33, 26-29 (1974).
26. A. I. Borisenko, O. N. Kostikov, and V. I. Chumachenko, Inzh.-Fiz. Zh., 24, No. 6, 1103-1108 (1973).
27. V. M. Buznik, G. A. Artemov, V. N. Bandura, and A. M. Fedorovskii, Inzh.-Fiz. Zh., 15, No. 5, 832-835 (1968).
28. V. M. Kas'yanov, Tr. MNI (Transactions of the Moscow Petroleum Institute), Issue 13, 145-151 (1953).
29. M. Murakami and K. Kikuyama, Trans. J. Fluids Engng., 102, No. 1, 97-103 (1980).
30. K. Nishibori, K. Kikuyama, and M. Murakami, JSME Int. J., 30, No. 206, 255-262 (1987).
31. K. Nishibori, K. Kikuyama, and N. Kakumn, Trans. JSME, Ser. B, 56, No. 525, 255-262 (1987).
32. Y. Yamada and S. Imao, Trans. JSME, Ser. B, 46, No. 409, 1662-1669 (1980).
33. Y. Yamada, S. Imao, and K. Toyozumi, Trans. JSME, Ser. B, 51, No. 461, 34-41, discuss. 41-42 (1985).
34. O. Zhang, S. Imao, M. Itoh, and Y. Yamada, Trans. JSME, Ser. B, 56, No. 525, 1321-1329 (1990).
35. J. N. Cannon and W. M. Kays, Trans. ASME, J. Heat Transfer, 91, No. 1, 135-140 (1969).
36. V. M. Kas'yanov, Tr. MNI (Transactions of the Moscow Petroleum Institute, Issue 11, 144-170 (1951).
37. S. Imao, Q. Zhang, and Y. Yamada, Trans. JSME, Ser. B, 54, No. 498. 243-248 (1988).
38. O. G. Martynenko, V. L. Kolpashchikov, and V. I. Kalilets, Convection in Channels [in Russian], Minsk (1971), pp. 3-42.
39. M. A. Mikheev, Fundamentals of Heat Transfer [in Russian], Moscow (1956).
40. F. Levy, Vereines Dentsch. Ing. Forschungsheft, No. 535, 18-45 (1929).
41. A. White, J. Mech. Eng. Sci., 6, No. 1, 47-52 (1964).
42. K. Nishibori, K. Kikuyama, M. Murakami, and T. Kimura, Trans. JSME, Ser. B, 53, No. 488, 1150-1156, discuss. 1157-1158 (1987).
43. M. Murakami, K. Kikuyama, K. Nishibori, and O. Kito, Mem. Fac. Eng. Nagoya Univ., 34, No. 2, 284-292 (1982).

44. M. Anwer and R. M. C. So, Exp. Fluids, 8, Nos. 1-2, 33-40 (1989).
45. D. J. Silvester, R. W. Thatcher, and J. C. Duthie, Computers and Fluids, 12, No. 41, 281-292 (1984).
46. M. A. Gol'dshtik and N. M. Ersh, Izv. Ross. Akad. Nauk, Mekh. Zhidk. Gaza, No. 2, 19-23 (1992).
47. E. L. Kaspin, Heat Transfer and Friction in Engines and Power-Generating Plants of Aircraft [in Russian], Kazan' (1987), pp. 32-38.
48. C. Y. Kuo, H. T. Iida, J. H. Taylor, and F. Kreith, Trans. ASME, J. Heat Transfer, 82, No. 2, 139-151 (1960).
49. S. Gilham, P. S. Ivey, J. M. Owen, and J. R. Pincombe, J. Fluid Mech., 230, 505-524 (1991).
50. I. N. Sidorov, Ya. D. Zolotonosov, G. N. Marchenko, and O. V. Maminov, Inzh.-Fiz. Zh., 54, No. 2, 198-202 (1988).
51. Y. Suematsu, T. Ito, and T. Hayase, Bull. JSME, 29, 258, 4122-4129 (1986).